Journal of the Meteorological Society of Japan, Vol. 72, No. 4, pp. 515–530, 1994

A Diagnostic Study of the Early Phases of Sixteen Western North-Pacific Cyclones

By Robert W. P. Kelly,[1] John R. Gyakum, Da-Lin Zhang, and Paul J. Roebber[2]

Department of Atmospheric and Oceanic Sciences, McGill University, 805 Sherbrooke Street West, Montreal, Quebec H3A 2K6, Canada

(Manuscript received 24 November 1993, in revised form 8 April 1994)

Abstract

We study the phenomenon of rapid cyclogenesis by examining the time evolution of the synoptic-scale environment for the 36-h period prior to most rapid intensification. We perform this study with the construction of composites for eight explosively-developing cyclones whose maximum intensification commences within a 5° latitude-longitude region in the vicinity of the Kuroshio Current. A comparison is made with corresponding composites of eight weakly-developing lows within the same region. The set of 16 cases is a comprehensive sample of events for nine cold seasons. Synoptic-scale features for the strong cases, distinct from those of the weaker cases, are detected throughout the 36-h dynamical conditioning period.

The stronger cases form to the south and west of Japan with antecedent propagation predominately over the maritime environment. The weaker systems, in contrast, either form *in situ* in our study region, or travel eastward from the Sea of Japan over the Island of Honshu. The unique thermodynamic precursors of the stronger systems include: a warm 1000–500 hPa thickness anomaly that travels from the East China Sea northeastward into the Kuroshio region, and a cold thickness anomaly and thermal jet east of our study area. The dynamical consequence of the warm anomaly includes the development of an anomalous southwesterly thermal wind to the northwest where incipient surface development occurs.

We examine a representative strong case in which initial surface development occurs to the northwest of the warm anomaly in a zone of quasi-geostrophic forcing for ascent. The system subsequently propagates into a favorable location for further development downstream of a second 500 hPa trough within the northwesterly polar jet. At the onset of explosive deepening, the cyclone is propagating towards a second region of anomalously cold air and strong baroclinity.

1. Introduction

The considerable research into explosive cyclogenesis (Sanders and Gyakum, 1980) in recent years has led to significant improvement in the prediction of cyclone track and intensity (see, *e.g.*, Sanders, 1992; Sanders and Auciello, 1989). Despite the improvements in forecasts of rapid cyclogenesis, the development of the more extreme events is often underforecast (Roebber, 1990). Furthermore, questions remain as to what processes, if any, are unique to more rapidly intensifying cyclones.

Recent research has suggested that the earlier phases of cyclogenesis may be crucial to the subsequent rapid intensification. For example, Kuo *et al.* (1991) found that the inclusion of surface heat fluxes in their model during the early stages of cyclogenesis over the east coast of the United States was critical in producing more successful, and more explosive, subsequent intensification. Gyakum *et al.* (1992), among others, have suggested that antecedent surface vorticity intensification feeds back positively on subsequent 24-h development by stretching in a cyclonically-enhanced environment.

Our objective is to document systematically, well-defined synoptic-scale features during the 36-h period prior to the onset of cyclogenesis in the western North-Pacific Ocean. Others, including Bell and Bosart (1989) and Sanders and Davis (1988) have successfully related large-scale circulation features to, respectively, the mesoscale processes of coastal frontogenesis and explosive cyclogenesis in the vicinity of coastal regions of North America. Our objective is met with an analysis of composite data taken

1 Current affiliation: United Kingdom Meteorological Office, Bracknell, Berkshire, England

2 Current affiliation: Department of Atmospheric Science, State University of New York at Albany, USA

from eight cases of weak cyclogenesis and eight cases of rapid cyclogenesis whose most extreme development is initiated in a 5 degree latitude-longitude region east of Japan. This area, located near the especially warm ocean current, the Kuroshio, is a region of climatologically active cyclogenesis. A nine-year period of cold-season (October through March) cyclogenesis is used to determine this sample of cyclones. These cases have been previously studied by Bullock and Gyakum (1993, hereafter referred to as BG) to determine synoptic-scale conditions; however, BG only examined large-scale conditions at the onset of most rapid intensification. The particular focus of this work is to systematically distinguish between ordinary and more rapid cyclogenesis as early as 36 h in advance of the event by identifying dynamical precursors specifically associated with each type.

This research examines specifically the time evolution of composite surface and upper-level fields for the 36-h period prior to most rapid cyclone intensification, and the interaction of such features. We also examine the distinctive dynamical characteristics of each class of cyclogenesis during this precyclogenetic period. The time evolution of each class of cyclone is examined in terms of 1000–500 mb thickness anomalies. The differences between the two composites will be examined both physically and statistically. Finally, more detailed dynamical analyses will be shown for a representative case of rapid cyclogenesis to support the conclusions made from the composite fields.

2. Methodology and organization

We consider a sample of 16 cyclones whose maximum intensification began within the region bounded by 35° to 40°N and 145° to 150°E. This particular region is enclosed by a box in the figures showing the composite and individual case analyses. This set of low pressure systems is chosen from the North-Pacific Ocean cyclone dataset as compiled by Gyakum *et al.* (1989). This data base consists of a life history of each cyclone that appeared on the 6-hourly National Meteorological Center (NMC) final manual analyses of the North-Pacific Ocean during the nine cold seasons (1 October through 31 March) from 1975–76 through 1983–84. An individual cyclone is used if it is surrounded by at least one closed isobar (4 mb contour interval) for at least one time. This low is then tracked throughout its life cycle from its first appearance until it loses its identity. This loss of identity typically occurs through a merger with other lows in the vicinity of the Aleutians or Kamchatka, at times considerably later than is considered in this study. Tabulations of each system's life cycle include analyzed position and central pressures of the surface cyclones at 0000 and 1200 UTC. Charts for 0600 and 1800 UTC are used in determining the continuity of each system. The 16 cases began their most rapid intensification in a region of the Kuroshio Current that has been shown by numerous climatological studies to have frequent cyclogeneses (see, *e.g.*, Sanders and Gyakum, 1980; Roebber, 1984; Chen *et al.*, 1992). These cases represent a subset of the 31-case sample described by BG. This larger sample comprises all surface cyclones whose maximum intensification begins in our study region. This study focuses on only those systems whose maximum deepening rates range from 0.56 to 0.98 Bergerons (11–19 hPa (24 h)$^{-1}$, hereafter referred to as strong non-bombs or SNs) and from 1.22 to 1.79 Bergerons (24–35 hPa (24 h)$^{-1}$, hereafter referred to as moderate bombs or MBs). The 24-h central pressure changes used above have been adjusted geostrophically to 45°N by

$$\Delta p_{45} = \Delta p_{\phi} \frac{\sin 45^{\circ}}{\sin \phi}, \tag{1}$$

where Δp_{45} is the adjusted pressure change, Δp_{ϕ} is the 24-h pressure change and ϕ is the latitude of the cyclone center 12 h after the onset of the 24-h period considered.

The 16-case sample therefore represents a comprehensive set of surface cyclones beginning their most rapid development in a region east of Japan for the 9 cold seasons ending 1983–84, of which 8 cases are characterized by relatively ordinary development and the other eight cases are considered to be rapidly developing systems. The mean maximum intensification of the MB case, as measured by central pressure fall, is approximately double that of the typical SN case. These SN and MB cases have been studied by BG only from the perspective of large-scale fields at the onset of most rapid development.

To examine these cases further, we use a second data set that is archived on the NMC octagonal grid, and compiled on a compact disk (Mass *et al.* 1987). This 47×51 grid of data consists of sea level pressure (SLP), 850 hPa geopotential height and temperature, and 500 hPa geopotential height and temperature, which are given at equally spaced points on a polar stereographic projection, true at 60°N, where the points are separated by a distance of 381 km.

The fields found from the NMC octagonal grid are composited for each of the 8-case SN and MB samples for the 36-h period prior to the time of onset of most rapid intensification (hereafter referred to as T_0). Missing grids for the 16-cases included the sea-level pressure field at T_0 in the SN case of December 1975 and the 500 mb field for the MB case of 1 February 1982 at $T_0 - 36$. While it should be expected that the compositing of cases in a fixed geographical region would minimize the smearing of synoptic-scale forcing mechanisms and preserve any topographic forcing processes, the compositing of features prior to T_0 may involve additional smear-

ing. Such additional smearing may be related to possible differing tracks of important transient features towards the region of maximum cyclogenesis at T_0. Therefore, we focus only on those features that are representative of each sample.

The work includes an examination of the time evolution of composite fields from the SN and MB samples, along with appropriate difference fields, in Section 3. A more detailed diagnostic study of one case from the MB sample is presented in Section 4. Conclusions follow in Section 5.

3. Composite fields

Figures 1a and 1b show the time evolution of the central pressures for the respective SN and MB samples during their life cycle. The contrast between the two samples is seen clearly in the enhanced life spans of MB before T_0 and after $T_0 + 24$ h. Though each sample is defined by their relative deepening rates between T_0 and $T_0 + 24$ h, the definitions do not explain directly the longer life of MB. The longer development period of MB prior to T_0 has been shown by Gyakum *et al.* (1992) to be possibly relevant in explaining the greater subsequent development. This idea is related to the examination of the frictionless vorticity equation in pressure coordinates in which the horizontal and vertical advections of vorticity, and the tilting of the horizontal components of vorticity into the vertical may be neglected in the vicinity of the cyclone center. These assumptions allow us to express this equation, valid at the surface cyclone center, as

$$\frac{d(\zeta + f)}{dt} = -(\zeta + f)\nabla \cdot \mathbf{V} \tag{2}$$

Expression (2) states that the increase in vorticity due to convergence is proportional to the convergence itself. Hence, greater antecedent vorticity development implies a greater vorticity at T_0, and a greater instantaneous cyclonic vorticity increase, for a given amount of convergence. This convergence may be associated with an interaction between an upper-level cyclonic vorticity maximum and the surface cyclone. Such an interaction would be expected to occur optimally during the 24-h period of most rapid intensification. A physical understanding of why this North Pacific MB sample consists of cyclones that typically develop for a longer time period before their maximum deepening is therefore crucial to understanding their greater subsequent intensification. Though the generally longer period of evolution for the MB sample after $T_0 + 24$ h is interesting, much of this later time period is characterized by either constant or gradually rising central pressures. Therefore, this study focuses on the early phases of these 16 cyclones.

The composite SLP and 1000–500 hPa thickness fields are shown for the SN and MB samples

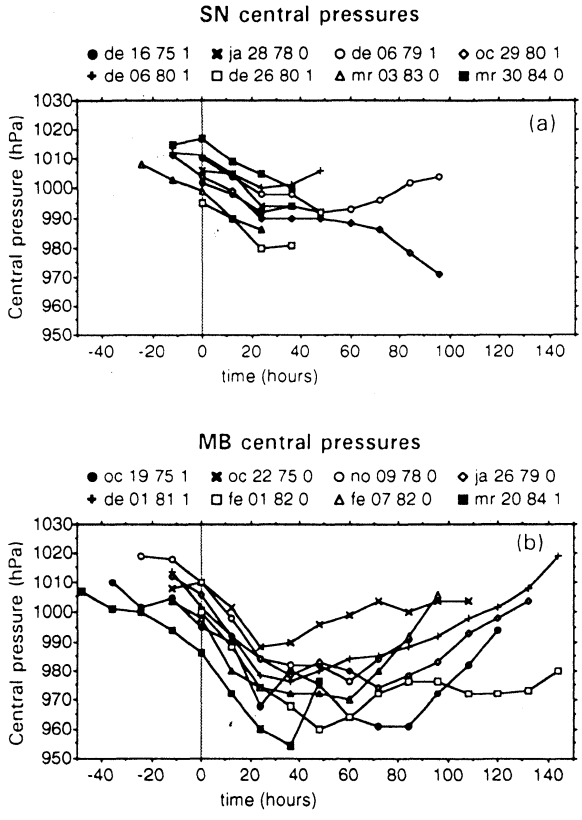

Fig. 1. Plots of central pressure (found from NMC manual analyses) as a function of time for each of the cyclones in the (a) SN and (b) MB samples, with 0 hours being T_0, the time of onset of the most rapid central pressure fall. Dates of each cyclonic system at T_0 are also shown, according to the convention of month, day, year, and time, where '0' corresponds to 0000 UTC and '1' corresponds to 1200 UTC.

in Figs. 2 and 3, respectively, with 12-h intervals from $T_0 - 36$ to T_0 hours. The thickness computation is accomplished by converting the SLP to 1000 hPa heights according to the standard conversion of 8 hPa $(6 \text{ dam})^{-1}$. The particularly noteworthy difference at T_0 is the more robust circulation for the composite MB cyclone than that for the SN composite, as could be expected from the generally longer development period of MB cases before T_0 (as shown in Fig. 1). To demonstrate this fact, we compute the maximum geostrophic vorticity associated with each composite low from the relation

$$\zeta_g = \frac{g}{f}\nabla^2 z, \tag{3}$$

where z is the 1000 hPa height. The central value of the MB cyclone at T_0 is 6.5×10^{-5} sec^{-1}, as opposed to the 3.1×10^{-5} sec^{-1} value of the SN center. This difference, along with the presence of the high

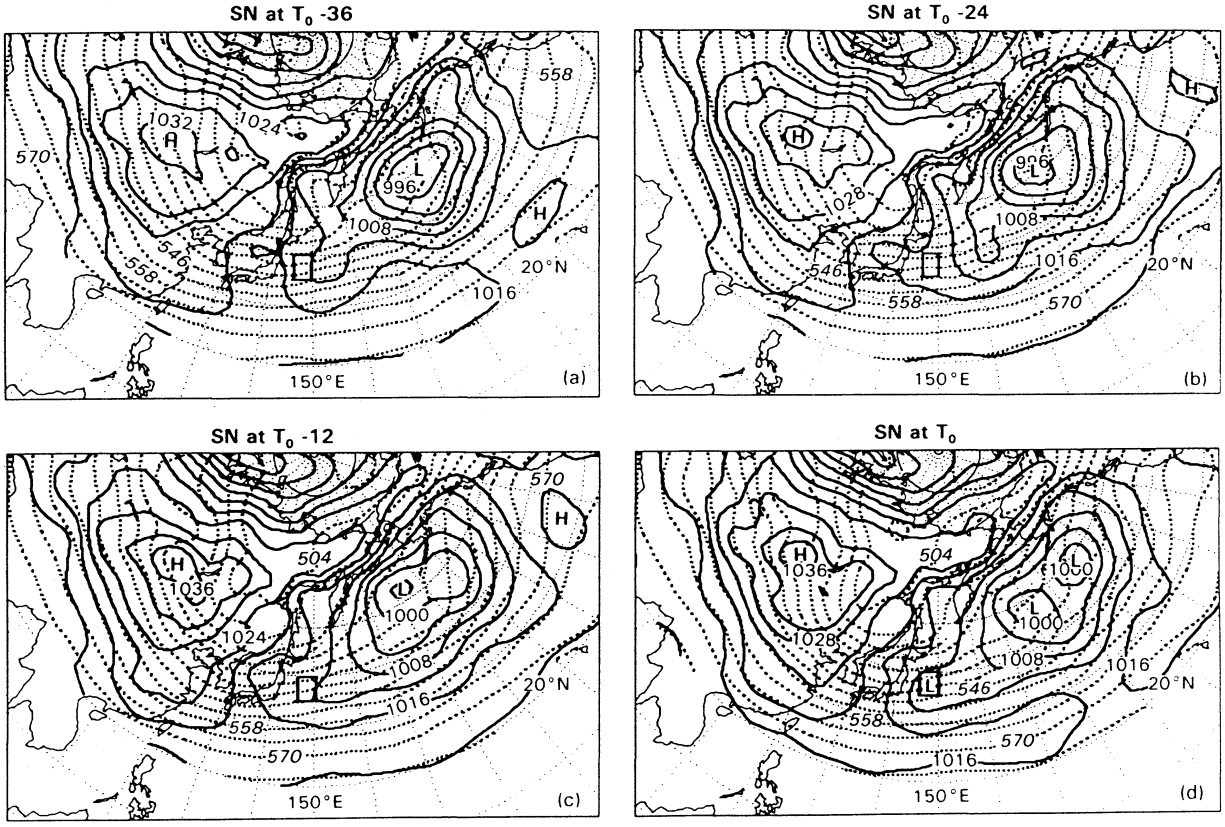

Fig. 2. Composite sea-level pressure (solid) at intervals of 4 hPa, and 1000–500 hPa thickness (dashed) at intervals of 6 dam, for sample SN at (a) $T_0 - 36$ h, (b) $T_0 - 24$ h, (c) $T_0 - 12$ h, and (d) T_0 h. The 5° latitude-longitude region of maximum cyclogenesis onset is shown by the box.

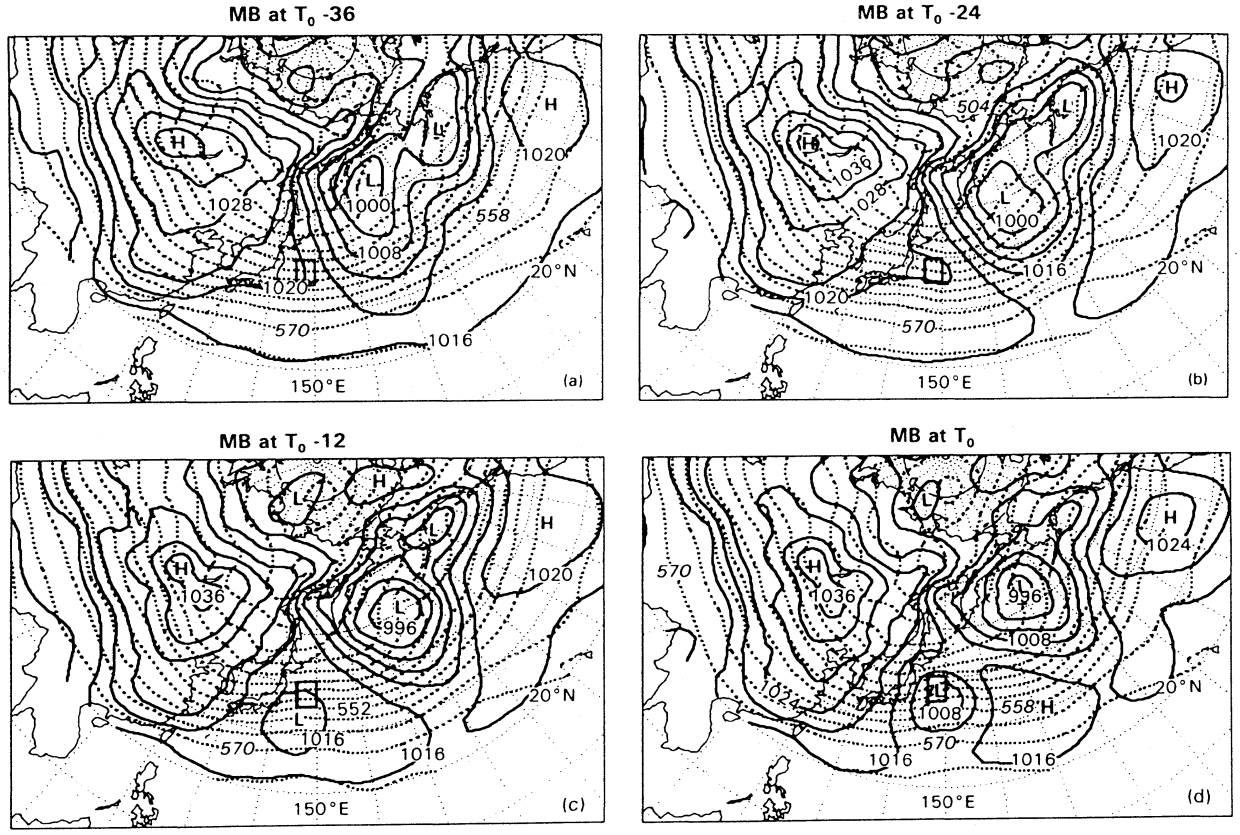

Fig. 3. As in Fig. 2, except for the sample MB.

pressure system (absent in the SN composite) to the east of the composite MB case, has been noted previously in the literature by BG. As will be discussed later, large vorticity maxima are more prevalent to the west of Honshu for earlier times in the SN cases, and the vorticity maxima for the MB cases are traceable to the south of Japan prior to T_0. What may be contributing to the more robust circulation for MB at T_0 is the fact that such vorticity maxima travel along a predominately marine trajectory. This issue will be discussed in more detail later in this section.

At $T_0 - 36$, both of the MB and SN composites are associated with a large Asian ridge, a feature that appears in long-term climatologies for the region (see, *e.g.*, Fig. 1.42 in Bluestein 1993). A difference between the two samples includes the stronger ridging in MB through Japan into the study region of the Kuroshio, with a suggestion of an inverted trough axis along the 135°E meridian south of Japan. Neither feature exists in either the SN field or in the long-term climatological fields. Another difference between the composites is the stronger surface downstream cyclonic circulation in MB maximized along the 170°E meridian southward from the composite center at 54°N, to the east of the Kamchatka Peninsula (southernmost point at 50°N, 157°E). This stronger downstream cyclone has an impact on the thickness pattern by producing a sharper downstream thermal jet and thickness trough along and equatorward of 40°N. The SN composite, in contrast, shows a deep surface cylone that is centered to the east of the dateline with its attendant circulation encompassing much of the northern part of the domain. The MB composite also shows a pronounced surface ridge offshore of California; such a ridge is present, though weaker, in the SN composite.

Throughout the next 36 h, the MB composite shows a strong surface ridge building to the southeast of Asia, during which time the inverted trough translates from the south of Japan and is seen as a closed cyclonic circulation by $T_0 - 12$ embedded within the larger-scale surface ridge. This pattern amplifies until T_0 when a separate downstream surface high is seen at 30°N, 170°E. In contrast, the SN composite cyclone at T_0 evolves from a trough that translates from the west, and is embedded in the large-scale low's circulation centered in the western part of the Aleutians. The structure of this Aleutian low differs from that of the downstream low in MB in that the SN system remains east of the dateline throughout the 36-h period. The downstream MB system, in contrast, just to the east of Kamchatka at $T_0 - 36$, has a stronger cold advection pattern south of 40°N that may be responsible for the stronger downstream thermal jet seen in the MB composite throughout the 36-h period.

Therefore, we conclude that the MB composite cyclone originates in an inverted trough from the south of Japan within a large surface ridge, a lobe of which builds southeastward from the Asian continent into Japan, and subsequently into the region of the dateline at 30°N by T_0. The SN composite, in contrast, is associated with a track farther north of cyclonic vorticity that crosses Japan during the 36 h antecedent period. The strong surface ridging, seen building southeastward through Japan in MB, is absent in the SN composite evolution. Figures 2 and 3 show that the large-scale cyclonic features can be traced backwards in time to $T_0 - 36$ h. However, the composite systems originate in two topographically different regions: the MB composite cyclone originates in the warm waters south of Japan and follows a maritime track into the Kuroshio Current region, and the SN composite originates over the Sea of Japan (Fig. 2a) with a subsequent eastward track through the Japanese island of Honshu.

To show the ensemble features suggested by our composites, we present the tracks of the individual low pressure centers, as shown on the manual analyses, in Fig. 4. The generally longer antecedent period of development for the MB cases is shown with predominately maritime tracks from the southwest into the region of most rapid development onset. This is consistent with our conclusions drawn from Fig. 3 in which the MB composite inverted trough follows a maritime trajectory from the southwest. The SN cyclones, in contrast, generally form *in situ* in the region of most rapid development onset. Generally, tracks of the MB cyclones subsequent to $T_0 + 12$ h, extend cyclonically into the region of the dateline poleward of 50°N, while those for SN extend only 200–400 km eastward (not shown).

To examine how representative the composite fields are of the respective samples, the relative vorticity maxima for each cyclone at T_0, are computed from the NMC gridded SLP field. The maximum geostrophic vorticity associated with the surface cyclone, is computed from equation 3. The vorticity maximum associated with each of the 16 cyclones is located at T_0 and then traced back in time to $T_0 - 36$ h. For a few cases, the vorticity maximum could only be traced back 12 or 24 h; this difficulty may have been due to the coarse resolution of the gridded data. Indeed Nielsen and Dole (1992), in their study of North American cyclones during the winter of 1986, have found that synoptic-scale cyclones often form as sub-synoptic scale features. Figure 5 shows the tracks of these cyclonic vorticity maxima for each sample of the cases. For MB, six of the eight cases could be tracked in from the southwest over maritime areas, one formed *in situ*, while only one tracked across Japan. This agrees with the MB composite SLP field (Fig. 3), which shows a ridge over Japan at $T_0 - 36$ and $T_0 - 24$

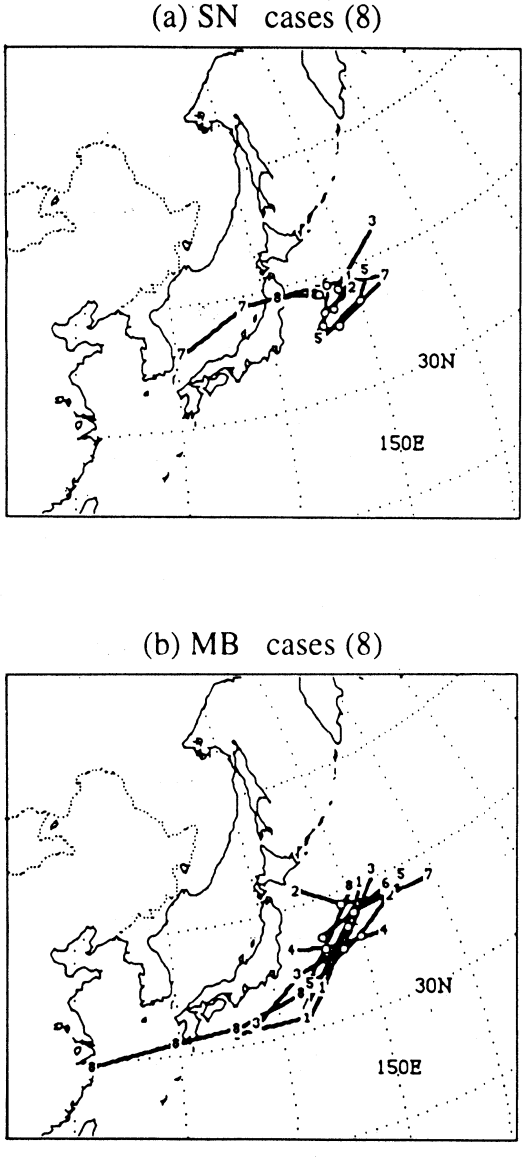

Fig. 4. Tracks of the eight cyclones of (a) SN and (b) MB from the time of their first formation (as analyzed on the NMC manual analyses) until $T_0 + 12$ h. The positions found on the analyses at T_0 are shown as open circles. Numbers shown are used for reference in tracking individual systems.

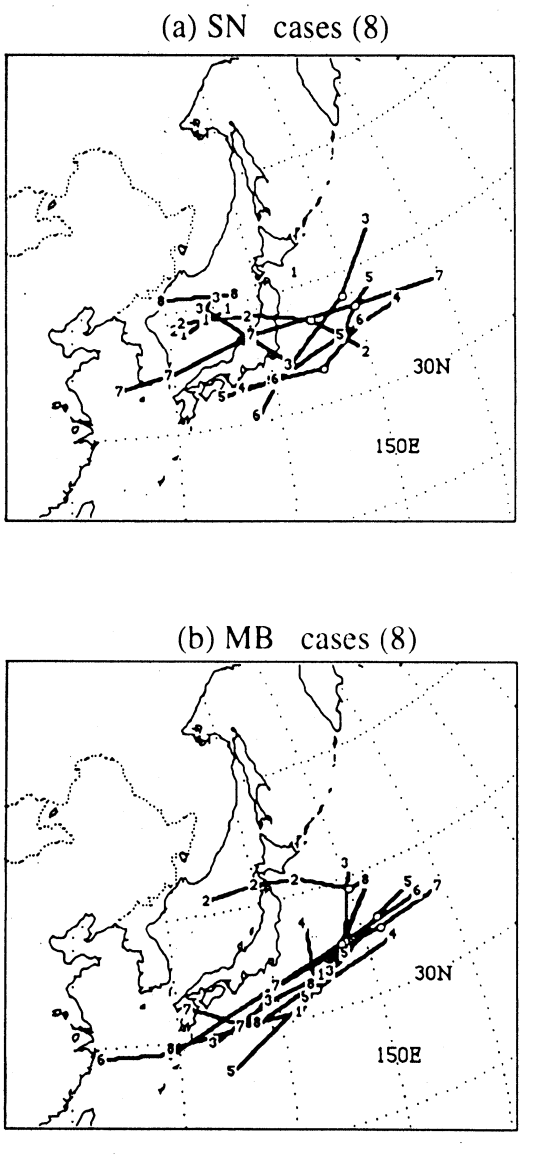

Fig. 5. Tracks of surface geostrophic relative vorticity maxima (computed from the NMC gridded SLP data) associated with the eight cyclones of (a) SN and (b) MB from $T_0 - 36$ h through $T_0 + 12$ h. The open circle denotes the position of the grid-point cyclonic vorticity maximum at T_0.

h forcing the baroclinic zone, and hence the storm track farther to the south over the open ocean. For the SN samples, only three cases could be tracked from the southwest, while five tracked across Japan. This is consistent with the SN composite SLP field (Fig. 2) which shows a cyclonic flow extending westward from the Aleutian low into the Sea of Japan. Figure 5 also shows a more coherent favored path for MB that is not apparent for the more dispersed cases of SN.

A comparison of Figs. 4b and 5b shows that the surface cyclone tracks and the grid-scale vorticity tracks are quite similar (though a small displacement is evident owing to the effect of the relatively coarse grid used to find the vorticity centers), whereas for SN (Figs. 4a and 5a) the vorticity tracks extend much farther westward than is shown for the individual cyclone tracks. This is because the MB cyclones form as distinct cyclones sooner than those of SN. Part of the reason for the later formation of the SN surface cyclones may be re-

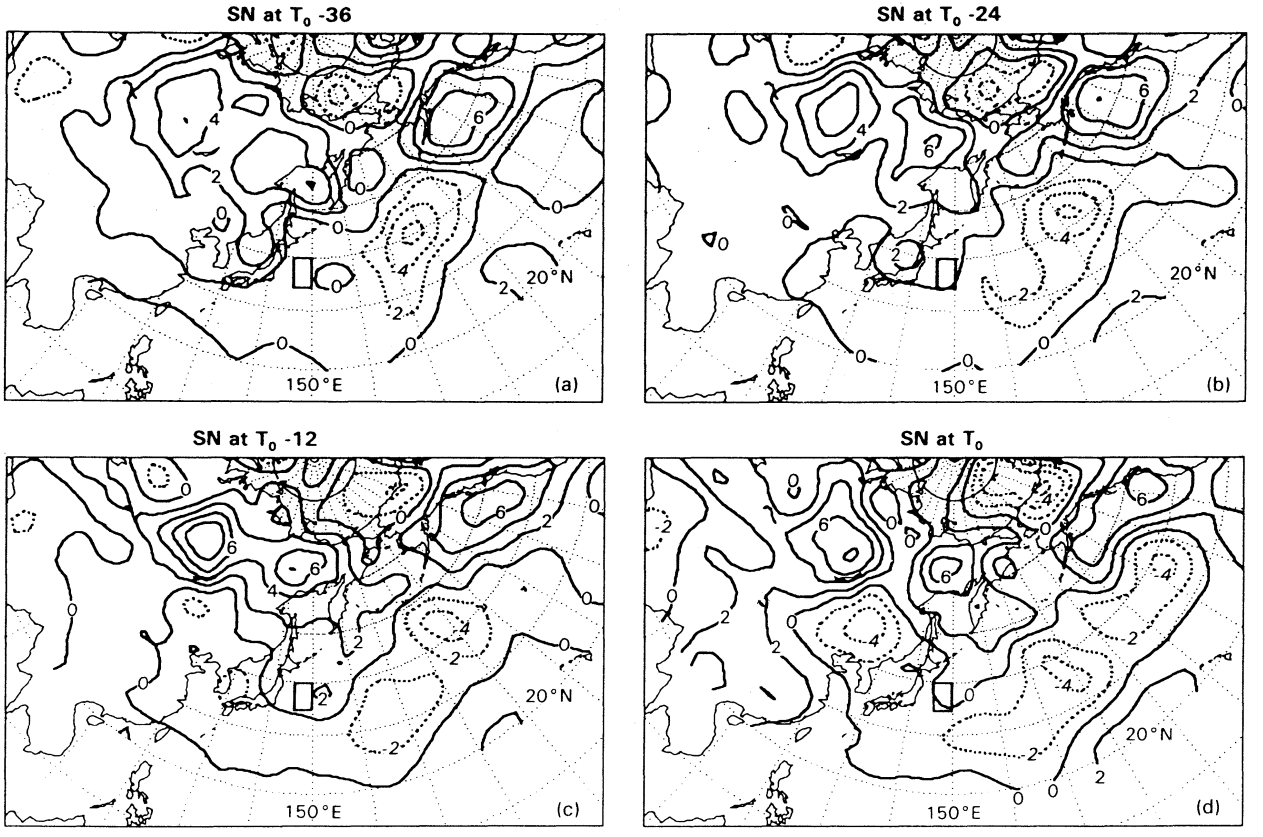

Fig. 6. Time evolution of composite 1000–500 hPa thickness anomalies at intervals of 2 dam for the SN sample of eight cyclones at (a) $T_0 - 36$ h, (b) $T_0 - 24$ h, (c) $T_0 - 12$ h, and (d) T_0 h. Solid (dashed) contours denote positive or zero (negative) values. The 5° latitude-longitude region of maximum cyclogenesis onset is shown by the box.

lated to the effects of the different grid-scale vorticity tracks. While the MB vorticity maxima generally have an unimpeded track across the warm waters of the Kuroshio Current, many of the SN cases track across the land mass of Japan. As these vorticity maxima track across Japan, the increased surface friction, decreased surface sensible heat and water vapor sources, and the considerable orography of Japan can all impede individual cyclone development. In fact, of the five SN cases in which the grid-scale vorticity maxima crossed Japan, only one is associated with a distinct cyclone that maintains its identity over the island. Three of the remaining four cases show vorticity maxima in the Sea of Japan that are also associated with manually-analyzed low pressure centers, but the vorticity maxima become associated with new individual systems east of Japan. The other SN case of a vorticity maximum, traceable across Japan, is not associated with a distinct surface low until after it passes across the island. These results are consistent with those of Chen *et al.* (1992) in which the authors suggest that the island of Honshu represents a less favorable environment for rapid cyclogenesis than either of the marine regions to its west and east.

To understand further the deep thermodynamic processes associated with each of the SN and MB samples, we display the time evolution of composite 1000–500 hPa thickness anomalies. Although we have seen the composite thickness fields in Figs. 2 and 3, the cases used range throughout the climatological cold period (*i.e.*, from October through the following March) with substantial seasonal change of thickness during this time. Therefore, we construct these anomalies by first establishing a 20-year 1000–500 hPa thickness climatology (1965–1984) for the appropriate half month in which a case occurs. We use only those days in which both 500 hPa and SLP fields are found. The percentage of times available for each half-monthly climatology range from 94.5% (586 of 620) for 16–31 October to 96.8% (600 of 620) for 16–31 January.

Figures 6 and 7, showing these anomalies for each of the respective SN and MB samples, reveal several distinct characteristics. The warm anomaly south of Japan at $T_0 - 36$ in MB follows closely the inverted trough seen in Fig. 3a. This anomaly translates slowly northeastward in the MB composite until it is

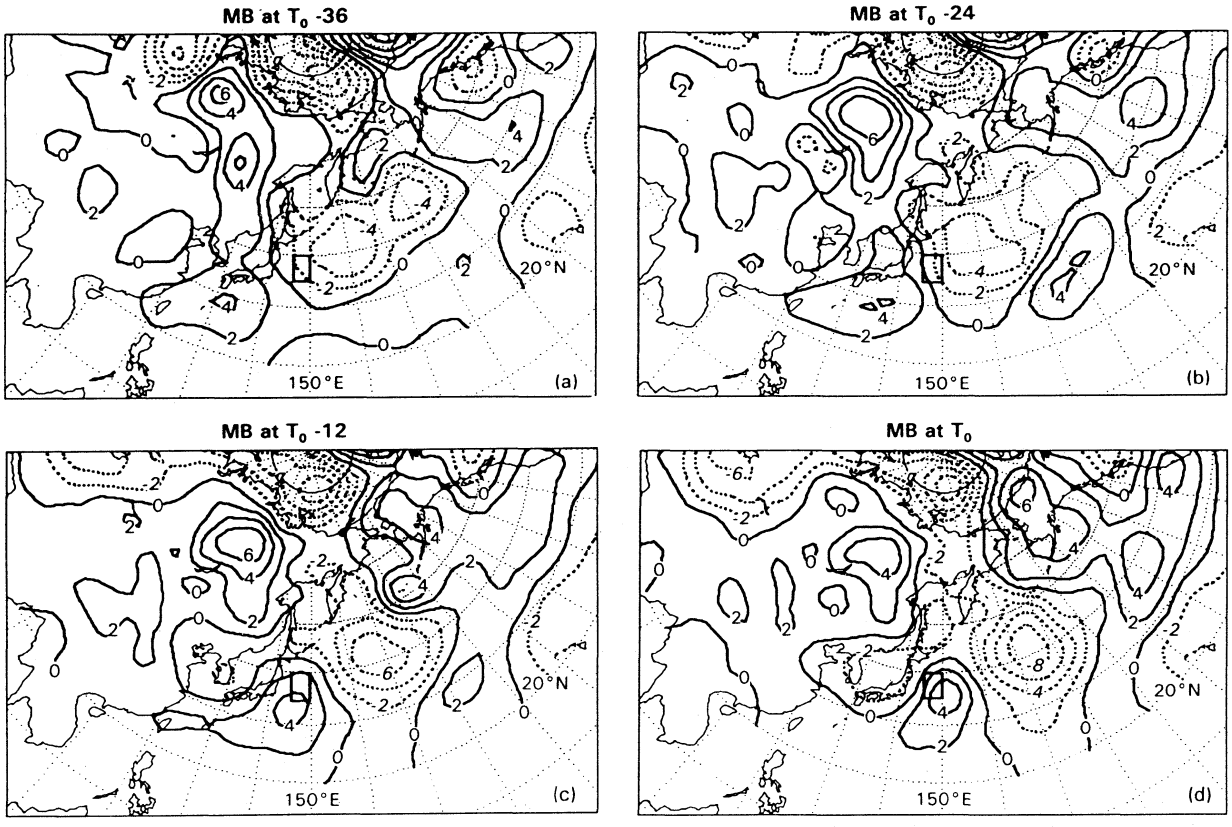

Fig. 7. As in Fig. 6, except for the sample MB.

located along the 150°E meridian (Fig. 7d) slightly to the east of the composite MB cyclone at T_0. Additionally, Fig. 7 shows a cold thickness anomaly in the MB composite that translates slowly eastward from 40°N, 158°E at $T_0 - 36$ h to 42°N, 173°E at T_0, having amplified to −10 dam (corresponding to a 4.9°C cold anomaly). This feature is associated with the strong cold advection pattern to the southwest of the deep composite low pressure center to the east of Kamchatka that translates eastward through the 36-h period (Fig. 3).

Furthermore, the combination of the warm anomaly slightly downstream of the composite MB surface low and the upstream cold anomaly west of Japan at T_0 produces an anomalously strong southwesterly thermal wind over the composite surface low. Figure 7 shows this anomalously strong flow to be traceable back in time to $T_0 - 36$ h, upstream of the composite inverted trough and warm anomaly seen in Fig. 3a. This is consistent with BG's conclusion of strong upper-level forcing for ascent in the vicinity of the MB composite. Here, we verify that such a conclusion is valid for as much as 36 h prior to T_0, with the feature primarily responsible being the warm anomaly. The pattern of the time evolution of the thickness anomaly in the SN composite (Fig. 6) shows none of the features just documented for the MB composite. Dynamically, the pattern is less favorable for development because of the SN composite's lack of particularly strong southwesterly thermal wind over the cyclone center at T_0, and the lack of an especially strong downstream thermal jet (baroclinity) that would be favorable for continued baroclinic development.

To emphasize the distinct features of the MB composite thickness anomalies, we show the 36-h time evolution of differences in the MB and SN anomalies in Fig. 8. This difference field appears similar to that shown for the MB field in Fig. 7. In fact, the warm anomaly of the MB composite to the south of Japan in the vicinity of the inverted trough at $T_0 - 36$ h (Fig. 3a) is sufficiently distinct from the sample of SN cases to show a statistically significant difference at the 95% confidence level, based upon a 2-sided student's t-test. The other region of significant difference at the 95% level, in the vicinity of the Hawaiian Islands is a zone of especially strong cold anomaly for the MB sample, in which surface ridging is evident (Fig. 3a). This region is shown to be statistically different throughout the subsequent time evolution through T_0 (Fig. 8). The warm anomaly south of Japan continues to show a statistically significant difference through T_0, though with less than 95% confidence at $T_0 - 12$. Additionally, the warm anomaly to the east of the downstream surface trough in the MB composite (see Figs. 3b

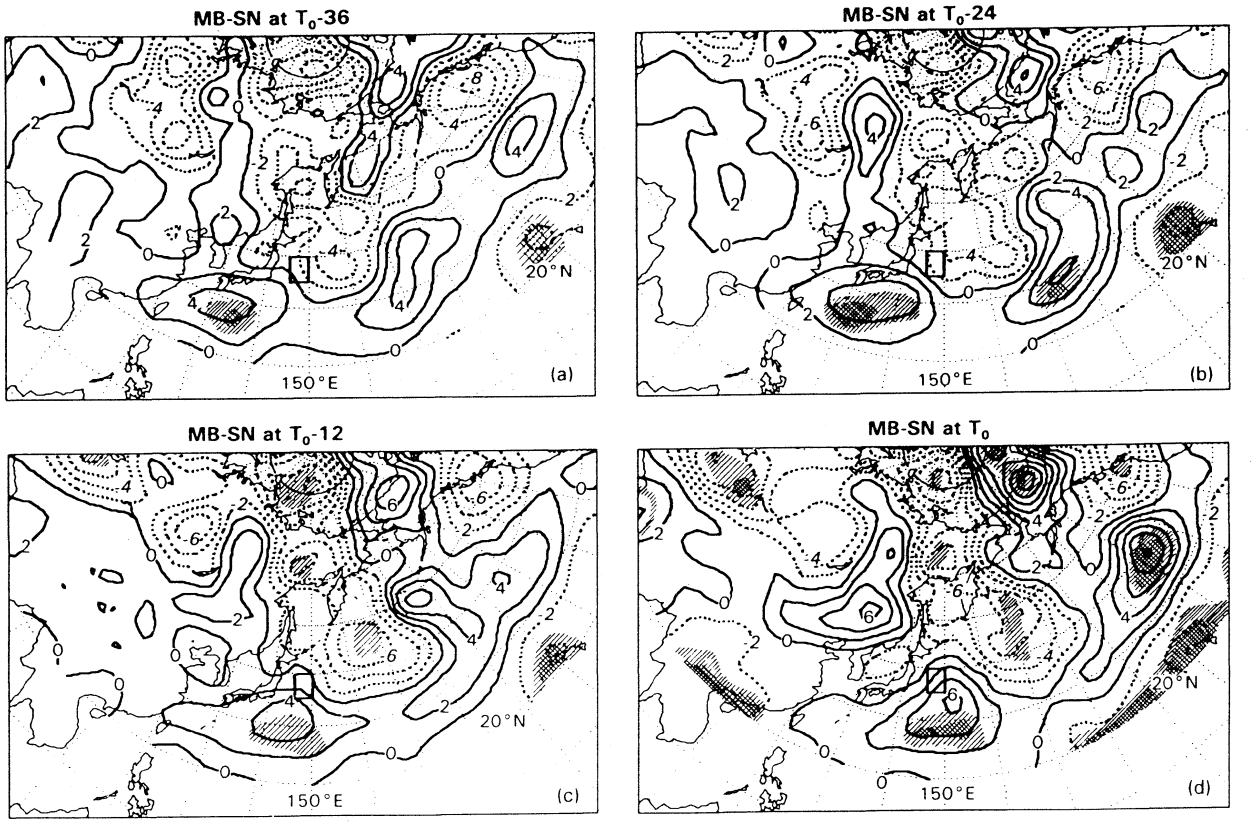

Fig. 8. Time evolution of the composite 1000–500 hPa thickness anomaly differences between the MB and SN samples. Solid (dashed) contours denote positve or zero (negative) values at intervals of 2 dam. Light shadings show regions in which the difference, based upon a 2-sided student's t-test, is statistically significant beyond the 90% confidence level. Dark shadings denote areas indicate regions with confidence levels in excess of 95%. The 5° latitude-longitude region of maximum cyclogenesis onset is shown by the box.

and 7b) is shown to survive the statistical test at the 95% confidence level (Fig. 8b). By $T_0 - 12$ h, the most significantly different region is related to the Hawaiian cold anomaly in the MB composite. The warm anomaly to the south and east of Japan is shown to be different from the SN sample only beyond the 90% confidence level. The cold anomaly to the southeast of Kamchatka (Fig. 7c), associated with the cold advection of the deep downstream composite surface low (Fig. 3c) is seen as being different from the SN sample beyond the 90% confidence level (Fig. 8c). At the onset of most rapid cyclone intensification, T_0, the downstream warm anomaly of the MB composite (Fig. 7d), associated with the warm advection pattern between the composite cyclone and the downstream surface ridge, is statistically different from that of SN at the 95% confidence level. The cold anomaly of the MB composite to the southeast of Kamchatka continues to be significant only beyond the 90% confidence level.

In summary, the MB warm anomaly, associated dynamically with the composite inverted trough and the anomalous southwesterly thermal wind prior to explosive development, is traceable at least 36 h prior to T_0; it is significantly different from the more benign sample of cyclones at the 95% confidence level. The downstream cold anomaly of MB, associated with the enhanced downstream thermal jet, is traceable throughout the 36-h period; it is also different from the SN sample (as early as $T_0 - 12$ h) beyond the 90% confidence level. Additional statistically significant differences, more numerous at T_0, and primarily in the eastern North Pacific, lend credence to the suggestion of a large-scale teleconnection pattern that is preferentially associated with the MB sample. For example, the 14 dam difference over Alaska is nearly collocated with a +8 dam maximum warm anomaly in MB (Fig. 7d) that is part of a large region of anomalously warm air.

4. Analysis of an MB case

We have documented statistically distinct deep tropospheric features of the MB sample that are not generally seen in a sample of more ordinary SN cases. Now, we show in more detail the dynamical features of a typical MB case that are associated

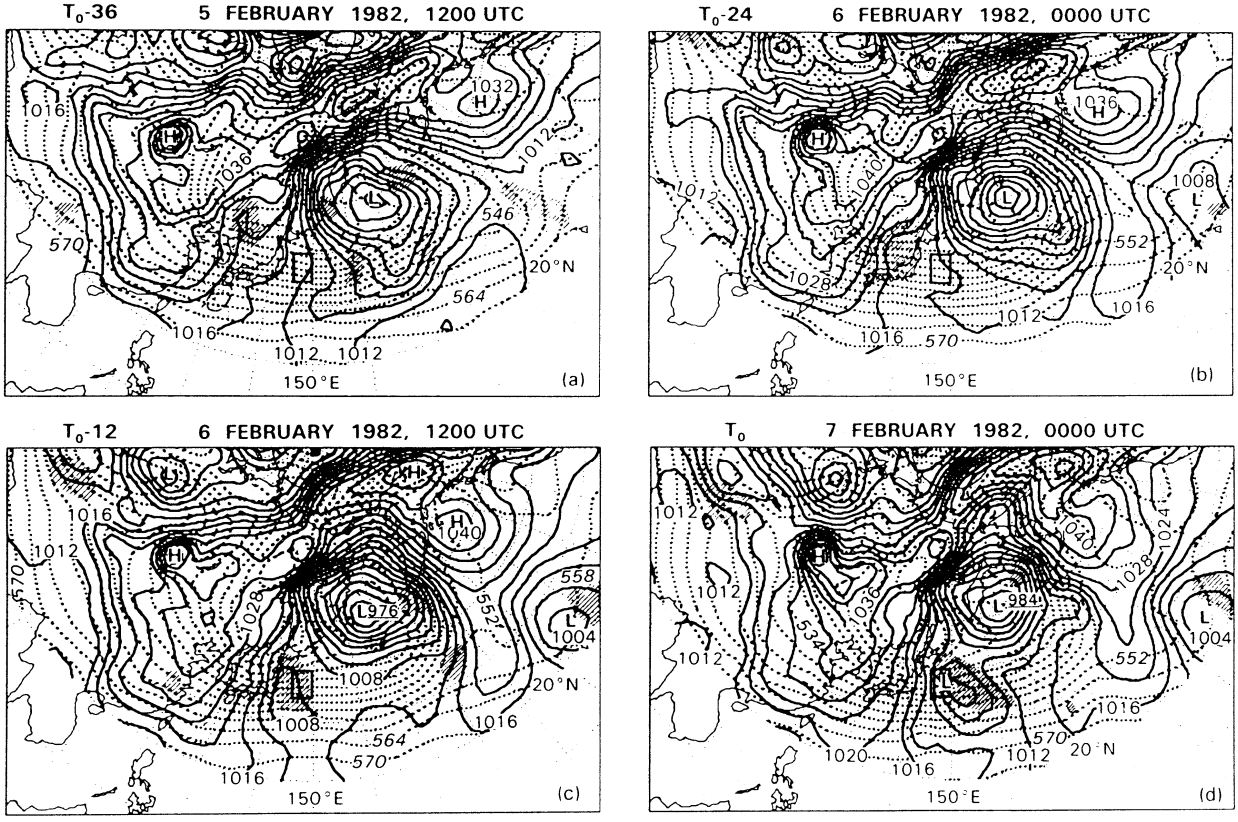

Fig. 9. Sea-level pressure field (solid) at intervals of 4 hPa and 1000–500 hPa thickness field (dashed) at intervals of 6 dam for an MB case at the times (a) $T_0 - 36$ h (1200 UTC 5 February 1982), (b) $T_0 - 24$ h (0000 UTC 6 February 1982), (c) $T_0 - 12$ h (1200 UTC 6 February 1982), and (d) T_0 h (0000 UTC 7 February 1982). Regions in which the term $2h\nabla \cdot \mathbf{Q}$ at 500 hPa is algebraically less than -5×10^{-16} hPa^{-1} sec^{-3} (forcing for quasi-geostrophic ascent) are shaded. The 5° latitude-longitude region of onset of maximum cyclogenesis is shown by the box.

with the unique thermodynamic anomalies shown in the MB composite.

To do so, we examine the quasi-geostrophic forcing of the w equation, as expressed as

$$\left(\sigma\nabla^2 + f_0^2\frac{\partial^2}{\partial p^2}\right)\omega = -2h\nabla\cdot\mathbf{Q} \tag{4}$$

where $\sigma = h\left(\frac{\partial\Theta}{\partial p}\right)$, where Θ is the potential temperature averaged on a constant pressure surface, $h = \left(\frac{R}{p}\right)\left(\frac{p}{p_0}\right)^{\kappa}$, κ is the ratio of the gas constant to the specific heat at constant pressure, p, and p_0 is 1000 hPa. The variable $\mathbf{Q}$ is a vector defined as

$$\mathbf{Q} = \left(-\frac{\partial\mathbf{V}_g}{\partial_x}\cdot\nabla\theta\right)\mathbf{i} + \left(-\frac{\partial\mathbf{V}_g}{\partial_y}\cdot\nabla\theta\right)\mathbf{j} \tag{5}$$

where $\mathbf{V}_g$ is the geostrophic wind, and $\nabla\theta$ is the horizontal potential temperature gradient. This form of the ω equation was introduced by Hoskins *et al.* (1978) and Hoskins and Pedder (1980). Quasi-geostrophic forcing for ascent and descent, is characterized, respectively, by convergence and divergence of $\mathbf{Q}$. A measure of geostrophic frontogenesis, G, is expressed as

$$G = \frac{\mathbf{Q}\cdot\nabla\theta}{|\nabla\theta|} \tag{6}$$

The forcing for ω is shown for 500 hPa and the function G is computed for the 850 and 500 hPa levels. Because of the limited vertical resolution of the data obtained from the compact disk, only quasi-geostrophic forcing for ω is computed, as any full solution for ω with such limited resolution would result in only crude estimates.

The case of 7 February 1982 at 0000 UTC (T_0) is selected in which the 24-h central pressure fall, according to (1), is −27.6 hPa. This pressure fall is near the median value for the sample of MB cases. The large scale conditions at $T_0 - 36$ include strong surface ridging throughout the eastern regions of Asia (Fig. 9a) with an associated axis of especially strong cold thickness anomaly extending through the Japanese islands (Fig. 10a). The −16 dam (−8°C) cold anomaly to the northwest of Japan (Fig. 10a) is associated with a digging 500 hPa cold trough in the northerly flow (Fig. 11a), where geostrophic frontogenesis in excess of 0.2 K (100 km)$^{-1}$ (3 h)$^{-1}$ is occurring in the confluent

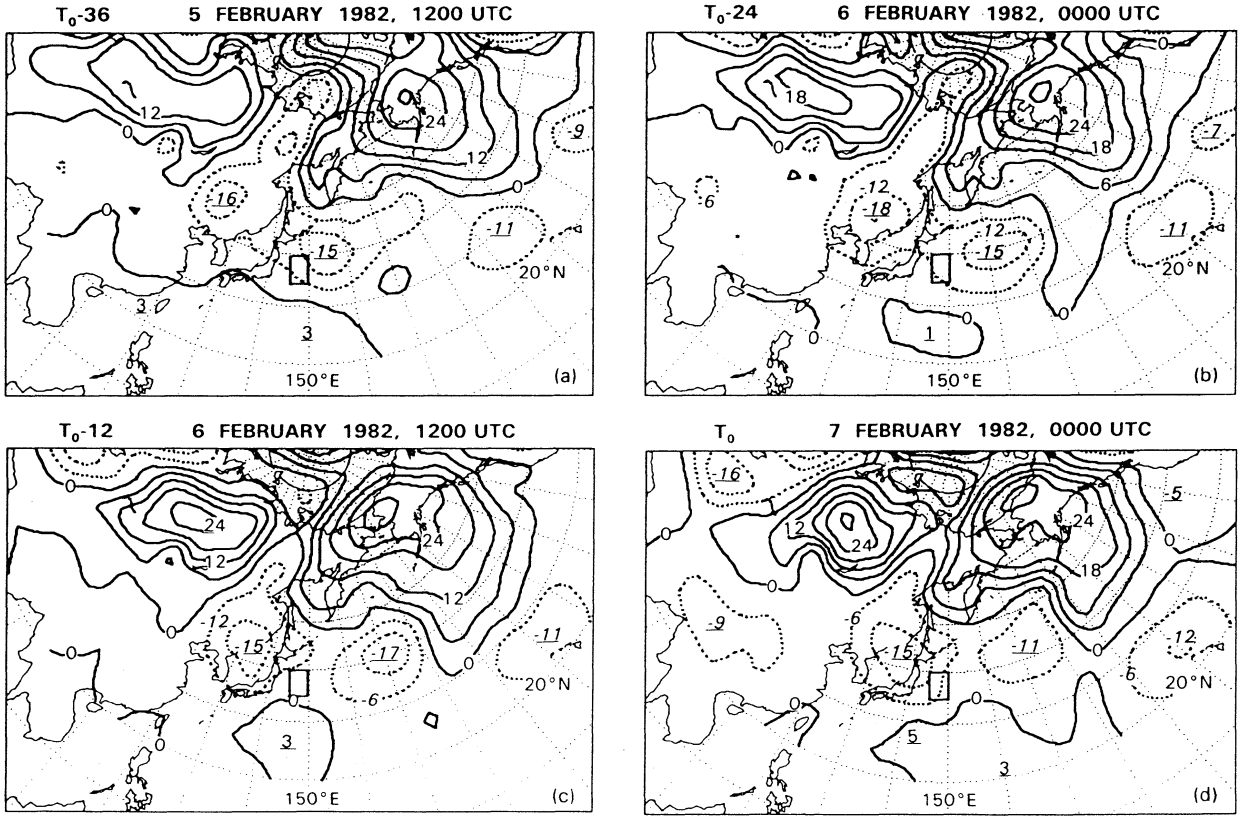

Fig. 10. Time evolution of 1000–500 hPa thickness anomalies (solid) at intervals of 6 dam for the MB case defined in Fig. 9 at (a) $T_0 - 36$ h, (b) $T_0 - 24$ h, (c) $T_0 - 12$ h, and (d) T_0 h. Solid (dashed) contours denote positive or zero (negative) values. The 5° latitude-longitude region of maximum cyclogenesis onset is shown by the box.

flow. This cold trough is also associated with a zone of enhanced 500 hPa Q vector convergence (maximum value of -12×10^{-16} hPa^{-1} sec^{-3}) and forcing for ascent (Fig. 9a). The −15 dam cold anomaly to the east of Japan (Fig. 10a) is associated with a region of strong cold advection to the southwest of a vigorous and large surface cyclone centered to the east of Kamchatka at 50°N, 170°E (Fig. 9a). The implication of these results is for an anomalously strong westerly thermal jet that extends from the area of interest to the dateline. The easternmost trough of the large 500 hPa vortex extends into the region of the Hawaiian Islands near 160°W where there is also anomalously cold air. There is a broad zone of anomalously warm air to the south of Japan in which a weak surface vorticity maximum develops near the southern tip of Japan at 32°N, 132°E, in the vicinity of which is a zone of weak 500 hPa forcing for ascent (light shading). This development is associated with a weak short wave at 500 hPa and anomalous southwesterly 1000–500 hPa thermal wind. At 850 hPa (Fig. 12a), the deep vortex southeast of Kamchatka provides strong cold advection southward to 25°N, and is associated with the offshore thickness anomaly (Fig. 10a). A suggestion of the surface trough is seen south of Japan with a secondary region of cold advection associated with the upstream digging trough and thickness anomaly.

At $T_0 - 24$ h, two sea-level cyclonic vorticity maxima are shown in Fig. 9b, one in the Sea of Japan near 38°N, 135°E that is directly associated with the amplifying cold pool in eastern Asia (Figs. 10b and 11b), and another to the south near 30°N, 135E° that is located downstream of a weak 500 hPa trough in anomalously strong southwesterly thermal wind. Upstream of these systems is an expanding zone of geostrophic frontogenesis (Fig. 11b) of maximum amplitude 0.3 K (100 km)$^{-1}$ (3 h)$^{-1}$. The zone of 500 hPa Q vector convergence (Fig. 9b) has enlarged to encompass much of northern Honshu, east of the more northern surface trough, and its maximum value has increased to -14×10^{-16} hPa^{-1} sec^{-3}.

By $T_0 - 12$ h, the southwesterly thermal wind anomaly has amplified (Fig. 10c) and a broad meridionally-oriented surface trough (Fig. 9c) has appeared to the east of Japan downstream of an amplifying 500 hPa trough (Fig. 11c). Upstream of this middle tropopsheric trough is the still-expanding region of geostrophically-forced frontogenesis. The individual, manually analyzed, surface system is seen

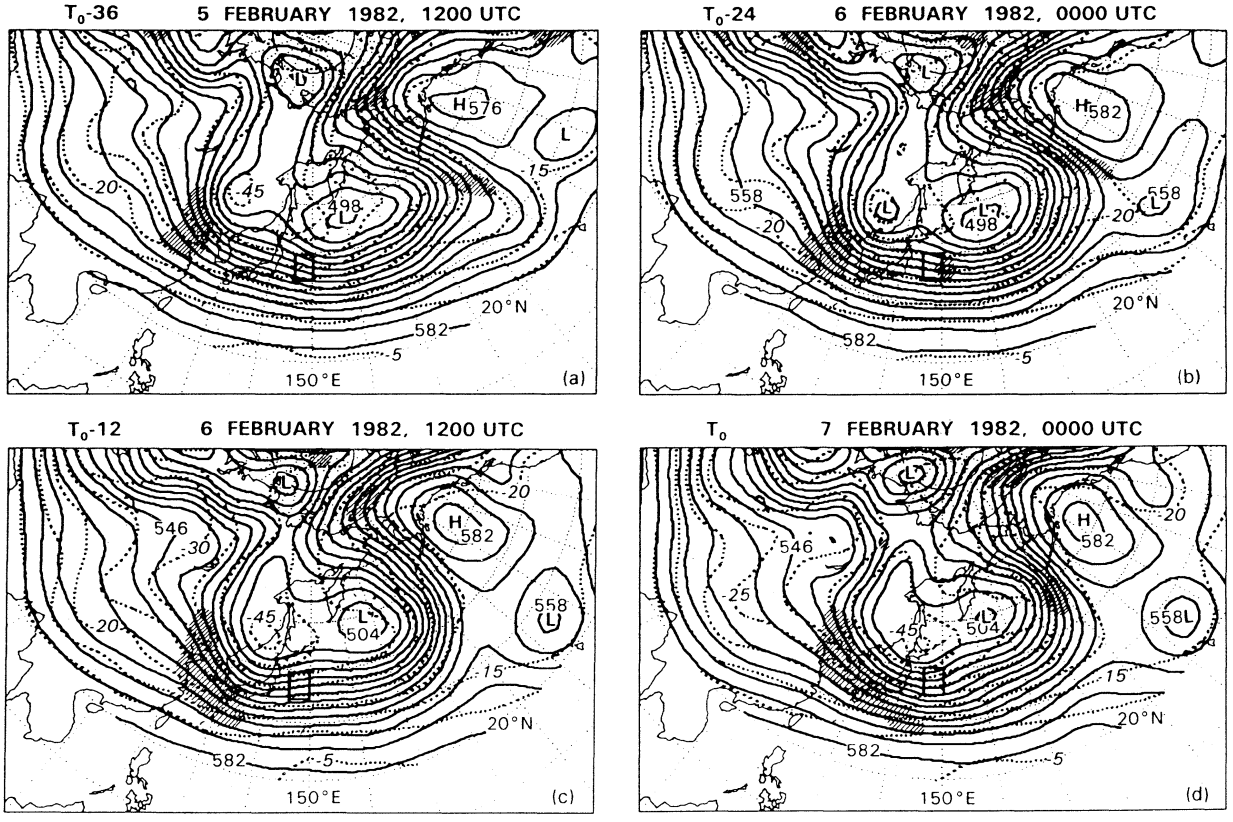

Fig. 11. Time evolution of 500 hPa heights (solid) at intervals of 6 dam and temperatures (dashed) at 5°C intervals, for the MB case defined in Fig. 9 at (a) $T_0 - 36$ h, (b) $T_0 - 24$ h, (c) $T_0 - 12$ h, and (d) T_0 h. Regions in which the geostrophic frontogenesis function $\frac{\mathbf{Q}\cdot\nabla\theta}{|\nabla\theta|}$ exceeds 0.2 K (100 km)$^{-1}$ (3 h)$^{-1}$ are shaded. The 5° latitude-longitude region of maximum cyclogenesis onset is shown by the box.

at 32°N, 143°E in the southern region of this trough in the anomalously warm air, though displaced to the northwest of its center (Fig. 10c). The 850 hPa field (Fig. 12c) shows an amplifying trough (along 145°E), associated with the surface low, which is traceable from the Asian continent. The deep surface cyclone to the east of Kamchatka (near 50°N, 165°E) continues to advect anomalously cold air, with an associated strong thermal jet, to the east of the incipient surface cyclone.

By T_0, the surface low has intensified by 6 hPa, propagated northeastward into the anomalously cold air at 38°N, 150°E (Fig. 10d), and continues to be located in a zone of strong 500 hPa Q vector convergence (Fig. 9d) that has expanded to the low's southeast. The cyclone, located downstream of the strong 500 hPa trough in a zone of Q vector convergence, is optimally placed for subsequent intensification. It is located 1000 km downstream of the −15 dam cold anomaly (Fig. 10d) and 1000 km to the northeast of an expanding region of 500 hPa frontogenesis (Fig. 11d). The system has intensified at 850 hPa to the extent that geostrophic frontogenesis in excess of 0.2 K (100 km)$^{-1}$(3 h)$^{-1}$ is shown in the expected regions of warm frontogenesis to the low's northeast and cold frontogenesis to the southwest.

To summarize, we find that upstream and downstream baroclinic amplification occurs at least 36 h in advance of the explosive cyclone deepening. At 850 hPa (Fig. 12), two separate baroclinic zones exist along the 120°E meridian at $T_0 - 36$ h. The southernmost zone is associated with the development of the surface vorticity maximum at 32°N, 132°E near a maximum of Q-vector convergence at 500 hPa (Figs. 9a). The second 850 hPa baroclinic zone is seen over the Asian continent in the vicinity of the large-scale trough near 47°N, 129°E. The temperature gradient in our study region sharpens and becomes more perturbed by T_0 as the second trough propagates southeastward to the east of Japan. The zones of Q-vector convergence move into a position east of Japan by T_0, after having amplified. Additionally, strong geostrophic frontogenesis at 500 hPa helps to strengthen the baroclinic zone to the west and south of Japan throughout the 36-h period.

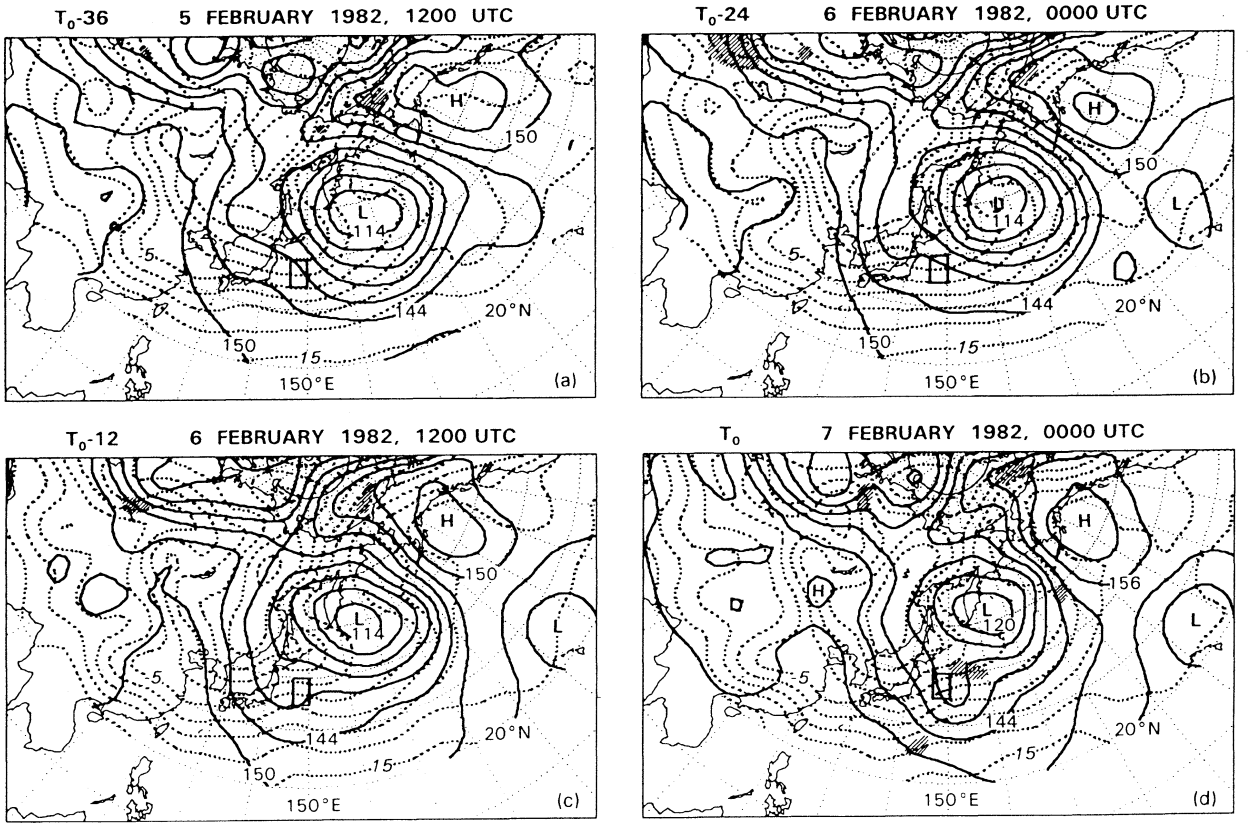

Fig. 12. As in Fig. 11, but for 850 hPa.

The frontogenesis that exists to the east of Japan throughout the antecedent period at 500 hPa, most prominently so at $T_0 - 24$ h (Fig. 11b) helps to condition the downstream environment. What is evident by T_0 is the surface cyclone, which is about to commence deepening explosively, is in the left exit region of a strong geostrophic jet and is upstream of another strong geostrophic jet. Such a pattern has been noted by other investigators for cases of rapid cyclogenesis (see, *e.g.*, Bell and Bosart 1988; and Uccellini and Kocin 1987). The life cycle of this cyclogenesis also is similar to that shown by Takayabu (1991) in which an initial lower tropospheric disturbance develops in warm air, and subsequently interacts with a well-developed upper trough associated with the polar jet. The conditioning processes detailed for this case of February 1982 mirror the large-scale features documented for the composite in the previous section.

5. Conclusions

This study examines thermodynamic and dynamic precursors to 16 cyclones whose maximum intensification begins in a 5° latitude-longitude region of the Kuroshio Current east of Japan, a climatologically active region of cyclogenesis. Eight of these systems were explosively developing (MB, with a range of 24-h central pressure falls from 24–35 hPa), while the other eight lows were non-explosively developing (SN, with a range of 24-h central pressure falls from 11–19 hPa). These cases represent a comprehensive set of surface lows that deepened for specified 24-h rates within the study area, for 9 years of cold seasons (1 October through 31 March). BG have documented large-scale differences between these two samples at time T_0. To determine the evolution of these distinct structures found by BG, we study the 36-h period prior to maximum development of each of these well-separated classes of cyclogenesis. Such a documentation may be important for forecasting, and for a more complete theoretical understanding of explosive cyclogenesis. Our conclusions from the composite study follow.

1) We find that the MB sample develops as an independent cyclonic disturbance within a region dominated by surface ridging that extends from the cold Asian anticyclone. The effect of this structure is to force the baroclinic zone equatorward into the warm, marine environment south and west of Japan. The MB lows typically propagate in this maritime region prior to their onset of maximum intensification at T_0.

2) The SN sample, in contrast, develops in a region dominated by a surface trough in the northerly flow behind the Aleutian low. An evaluation of individual surface low tracks (Fig. 4a) shows that the

SN cases typically developed *in situ* at T_0 in the Kuroshio region. Of the five cases with grid-scale vorticity maxima originating in the Sea of Japan (Fig. 5a), only one is associated with a manually-analyzed surface cyclone whose identity could be traced across the island.

3) Our finding of the differing tracks of each sample support BG's conclusion that the surface geostrophic vorticity of the MB sample at T_0 exceeds that of SN. The MB sample is influenced by weaker frictional effects of land, weaker hydrostatic stability and the abundance of moisture and heat fluxes from the underlying ocean.

4) Having constructed 1000–500 hPa thickness anomalies for each sample, we find the MB anomaly field to be characterized by two prominent feaures that are traceable throughout the 36-h period prior to T_0. The first feature is a warm anomaly that follows closely the ensemble tracks of the MB systems. Its mean amplitude exceeds 4 dam throughout the period. The second feature is an anomalous cold pool with an amplitude exceeding 8 dam at T_0, centered east of our study region, and associated with strong cold advection in the wake of a deep and large cyclone near Kamchatka.

5) The dynamical importance of the first feature is the anomalous southwesterly thermal winds are associated with the MB lows. Since the warm anomaly lies to the south and east of the composite surface low, our finding is similar to that of Sanders and Davis (1988), who found that anomalous southwesterly thermal wind exists in the vicinity of a larger sample of North Atlantic cases. Their study, however, focused on the importance of a planetary-scale cold pool of thickness anomaly in determining such an anomalous thermal wind.

6) The possible dynamical importance of the second feature is that the downstream thermal jet is being enhanced prior to the maximum cyclone intensification. The surface cyclone thus begins its explosive development downstream of an anomalous southwesterly thermal wind, and upstream of a second enhanced jet.

7) The SN composite anomaly fields, in contrast, show no such features. In fact, a statistical examination of the individual cases show that the upstream warm anomaly, found in MB, is significantly different from that of SN, at the 95% confidence level as early as $T_0 - 36$ h. The cold anomaly field is found to be significantly different from that of SN, beyond the 90% confidence level as early as $T_0 - 12$ h. A surprising result of this study is that only a 3 dam cold pool is found in the MB-SN difference field over the Sea of Japan. The dominant contribution to the anomalous southwesterly thermal wind over the low center in MB is, therefore, the warm pool that is detectable 36 h prior to T_0.

8) The documentation of a warm thickness anomaly 36 h before T_0 is important, because it is typically associated with early surface trough development. Additionally, this anomaly, when combined with the approaching upper trough (*e.g.*, Figs. 7d, 10d and 11d), helps to increase the upper-level forcing for cyclogenesis.

We show a representative MB case of 7 February 1982, supporting the findings of the composite analysis, in which such thickness anomalies are present. These anomalies are related to such quasi-geostrophic dynamical precursors as frontogenesis and forcing for ascent. The surface environment, near the warm thickness anomaly, is conditioned by weak surface vorticity spinup related to a subtropical trough with weak forcing for ascent. Subsequent to this time, a digging polar trough translates southeastward into the region of the Kuroshio and spins up this moist system explosively. The upstream environment at 500 hPa is characterized by an expanding region of frontogenesis that is active throughout the 36-h period prior to T_0. By T_0, the surface system is developed sufficiently so that both warm and cold frontogenesis zones are easily detectable at 850 hPa. Downstream of the incipient system, a deep surface cyclone east of Kamchatka, advects cold air as far south as 25°N. Such conditioning acts to amplify the downstream thermal jet, so that the low at T_0 is positioned optimally downstream of one trough, and in the right entrance region of another jet.

The identification of such favorable large-scale dynamic precursors in the MB sample, with a well-defined upper trough triggering explosive intensification, is consistent with the theoretical work by Farrell (1985) in which cyclogenesis can be treated as an initial-value problem with substantial growth of non-modal waves. Our findings of an upper-level trough being crucial to rapid cyclogenesis mirror those of Sanders (1986) for a sample of cases in the western North Atlantic Ocean. However, our documentation of the distinct downstream warm and cold anomaly precursors to rapid cyclogenesis (Fig. 8d), which define this middle-tropospheric forcing, suggests that future research focus on the evolution of such features.

Acknowledgments

This work has been supported by a subvention from the Atmospheric Environment Service of Canada, the Canadian Natural Sciences and Engineering Research Council under operating Grant P0037433, and the United States National Science Foundation under Grants ATM-8516263 and ATM-8814816. Drafting assistance has been provided by Ms. Ursula Seidenfuss. Support for the lead author's (RWPK) Master's Degree study has been provided by the Canadian Commonwealth Scholarship Programme.

References

Bell, G.D. and L.F. Bosart, 1989: The large scale atmospheric structure accompanying New England coastal frontogenesis and associated North American cyclogenesis. *Quart. J. Roy. Meteor. Soc.*, **115**, 1133–1146.

Bluestein, H.B., 1993: Synoptic-Dynamic Meteorology in Midlatitudes, Volume II: Observations and Theory of Weather Systems, Oxford University Press, 594 pp.

Bullock, T.A. and J.R. Gyakum, 1993: A diagnostic study of cyclogenesis in the western North Pacific Ocean. *Mon. Wea. Rev.*, **121**, 65–75.

Chen, S.-J., Y.-H. Kuo, P.-Z. Zhang and Q.-F. Bai, 1992: Climatology of explosive cyclones off the East Asian coast. *Mon. Wea. Rev.*, **120**, 3029–3035.

Farrell, B., 1985: Transient growth of damped baroclinic waves. *J. Atmos. Sci.*, **42**, 2718–2727.

Gyakum, J.R., J.R. Anderson, R.H. Grumm and E.L. Gruner, 1989: North Pacific cold-season surface cyclone activity: 1975 through 1983. *Mon. Wea. Rev.*, **117**, 1141–1155.

Gyakum, J.R., P.J. Roebber and T.A. Bullock, 1992: The role of antecedent surface vorticity development as a conditioning process in explosive cyclone intensification. *Mon. Wea. Rev.*, **120**, 1465–1489.

Hoskins, B.J. and M.A. Pedder, 1980: The diagnosis of midlatitude synoptic development. *Quart. J. Roy. Meteor. Soc.*, **106**, 707–719.

Hoskins, B.J., I. Draghici and H.C. Davies, 1978: A new look at the omega-equation. *Quart. J. Roy. Meteor. Soc.*, **104**, 31–38.

Kuo, Y.H., R.J. Reed and S. Low-Nam, 1991: Effects of surface energy fluxes during the early development and rapid intensification stages of seven explosive cyclones in the western Atlantic. *Mon. Wea. Rev.*, **119**, 368–384.

Mass, C.F., H.J. Edmon, H.J. Friedman, N.R. Cheney and E.E. Recker, 1987: The use of compact discs for storage of large meteorological and oceanographic datasets. *Bull. Amer. Meteor. Soc.*, **68**, 1556–1558.

Nielsen, J.W. and R.W. Dole, 1992: A survey of extratropical cyclone characteristics during GALE. *Mon. Wea. Rev.*, **120**, 1156–1167.

Roebber, P.J., 1984: Statistical analysis and updated climatology of explosive cyclones. *Mon. Wea. Rev.*, **112**, 1577–1589.

Roebber, P.J., 1990: Variability in successive operational model forecasts of maritime cyclogenesis. *Wea. Forecasting*, **5**, 586–595.

Sanders, F., 1986: Explosive cyclogenesis in the west-central North Atlantic Ocean, 1981–84. Part I: Composite structure and mean behavior. *Mon. Wea. Rev.*, **114**, 1781–1794.

Sanders, F., 1992: Skill of operational dynamical models in cyclone prediction out to five-days range during ERICA. *Wea. Forecasting*, **7**, 3–25.

Sanders, F. and J.R. Gyakum, 1980: Synoptic-dynamic climatology of the "bomb." *Mon. Wea. Rev.*, **108**, 1589–1606.

Sanders, F. and C.A. Davis, 1988: Patterns of thickness anomaly for explosive cyclogenesis over the west central North Atlantic Ocean. *Mon. Wea. Rev.*, **116**, 2725–2730.

Sanders, F. and E.P. Auciello, 1989: Skill in prediction of explosive cyclogenesis over the western North Atlantic Ocean, 1987/88: A forecast checklist and NMC dynamical models. *Wea. Forecasting*, **4**, 157–172.

Takayabu, I., 1991: "Coupling development": An efficient mechanism for the development of extratropical cyclones. *J. Meteor. Soc. Japan*, **69**, 609–628.

Uccellini, L.W. and P.J. Kocin, 1987: The interaction of jet streak circulations during heavy snow events along the East Coast of the United States. *Wea. Forecasting*, **2**, 289–308.

西北部太平洋における低気圧の発達初期の診断研究

R.W.P. Kelly • J.R. Gyakum • D.-L. Zhang • P.J. Roebber

(Department of Atmospheric and Oceanic Sciences McGill University, Canada)

本研究では、低気圧の爆発的な発達の実態を明らかにするために低気圧の発達期前の 36 時間について総観場の時間変化の事例解析を行なった。黒潮領域付近の 5°緯度・経度グリッド内で急激に発達した低気圧(爆発的低気圧) 8 例について解析し、そのコンポジットを作成した。比較のために、同一領域で穏やかに発達した別の 8 例の低気圧についてもコンポジットを作成した。本研究で解析された事例の総数は寒候期 9 年分についての 16 例である。爆発的低気圧と穏やかに発達するものとでは、発達期前の 36 時間の総観場の力学的特性に顕著な差が見られた。

爆発的低気圧は日本の南方から西方で形成され、海洋上を東に移動してゆく。それに対し、穏やかに発達するものは本研究の解析領域で形成されるか、あるいは日本海から本州を通過して東に抜けることが多い。爆発的低気圧となる特徴的な熱力学的前兆として、東シナ海からその北東の黒潮領域へ移動する

1000–500 hPa の層厚の正のアノマリや本研究の解析領域の東側の層厚の負のアノマリとそれに付随する熱的ジェット気流、などがあげられる。層厚の正のアノマリの結果その北西部で強い南西温度風が形成され、そこの大気下層で初期の発達がみられる。

本研究では、下層での初期の発達が層厚の正のアノマリの北西で生じた爆発的低気圧の代表的なケースについて調べた。この発生領域には準地衡風的強制により上昇流が生じている。ここで発生した低気圧は、より発達しやすい環境にある北西寒帯ジェット下流の 500 hPa 面の第 2 のトラフ域へと流れて行く。そして、この低気圧が強い傾圧性をしめす第 2 の寒気領域に移動して行くと、爆発的な気圧の低下が始まることを明らかにした。